

Catching Spiral - S0 transition in groups. Insights from SPH simulations with chemo-photometric implementation

P. Mazzei^a, A. Marino^b, R. Rampazzo^a, G. Galletta^b, D. Bettoni^a

^a*INAF-Osserv. Astronomico di Padova, Vic. dell'Osservatorio 5, 35122 Padova, Italy*

^b*Dip. di Fis. ed Astron. "Galileo Galilei", Vic. dell'Osservatorio 3, 35122, Padova, Italy*

Abstract

We are investigating the co-evolution of galaxies within groups combining multi-wavelength photometric and 2D kinematical observations. Here we focus on S0s showing star formation in ring/arm-like structures. We use smooth particle hydrodynamical simulations (SPH) with chemo-photometric implementation which provide dynamical and morphological information together with the spectral energy distribution (SED) at each evolutionary stage. As test cases, we simulate the evolution of two such S0s: NGC 1533 and NGC 3626.

The merging of two halos with mass ratio 2:1, initially just composed of DM and gas, well match their observed SEDs, their surface brightness profiles and their overall kinematics. The residual star formation today “rejuvenating” the ring/arm like structures in these S0s is then a mere consequence of a major merger, i.e. this is a phase during the merger episode. The peculiar kinematical features, e.g. gas-stars counter rotation in NGC 3626, depends on the halos initial impact parameters. Furthermore, our simulations allow to follow, in a fully consistent way, the transition of these S0s through the green valley in the NUV–r vs. M_r colour magnitude diagram, which they cross in about 3-5 Gyrs, before reaching their current position in the red sequence. We conclude that a *viable* mechanism driving the evolution of S0s in groups is of gravitational origin.

Keywords: Galaxies: evolution, Galaxies: interactions, Galaxies: individual: NGC 3626, NGC 1533, Method: numerical

1. Introduction

The investigation of the co-evolution of galaxies and groups in the nearby Universe is of great cosmological interest since more than half of galaxies reside in groups. Since the velocity dispersion of galaxies in groups is low, i.e. comparable to the stellar velocity dispersion, mergers of galaxies are highly favoured with respect to clusters. Nearby groups provide a close-up view of phenomena driving the morphological and star formation (SF) evolution of galaxy members before they fall into clusters (e.g. [Boselli & Gavazzi, 2006](#); [Wilman et al., 2009](#); [Just et al., 2010](#)).

Among open questions, the old controversy about the *nature* vs. *transformation* origin of S0 galaxies rises above the others. Since Es and S0s are the typical inhabitants of nearby clusters, at expense of Spirals (Sps), a debate about the transformation of Sps into S0s in such environments arose.

The processes possibly driving the Sp→S0 transformation are, indeed, still uncertain and debated (e.g. [Bekki, 2009](#)). They include feedback from AGN ([Schawinski et al., 2009](#)) which may shut down SF, environmental effects which reduce the HI reservoir of Sps, ([Boselli & Gavazzi, 2006](#); [Hughes & Cortese, 2009](#); [Cortese & Hughes, 2009](#)) and the interplay between cold gas flows and shock heating ([Dekel & Birnboim, 2006](#)). [Wetzel et al. \(2012\)](#) find that galaxies in groups and clusters experience no significant environmental effects until they cross within the virial radius of a more massive host halo. [Boselli & Gavazzi \(2006\)](#) claim that the interaction with the intergalactic medium is not the origin of the cluster S0s, which likely form by Sps through gravitational interaction. Studying 116 X-ray selected galaxy groups at redshift 0.2-1, [George et al. \(2013\)](#) conclude that strangulation and disk fading are insufficient to explain the observed morphological dependence on environment, and that galaxy mergers or close tidal encounters must play a role in building up the population of quenched galaxies with bulges seen in dense environments at low redshift.

The comparison of clusters at $z \approx 0.1 - 0.2$ with some at intermediate distance, $z \approx 0.4 - 0.5$, shows that a sort of morphological conversion in the galaxy population from Sps→S0s took place about 1 - 4 Gyr ago ([Fasano et al., 2000](#)). This transformation anti-correlates with the local density, i.e., in low concentration clusters the transformation happened only about 1-2 Gyr ago.

The effects of the possible galaxy morphological transformation manifest themselves also in the nearly ubiquitous bimodal distribution of galaxies in

the colour-magnitude diagram (CMD) (e.g. [Strateva et al., 2001](#); [Lewis et al., 2002](#); [Baldry et al., 2004](#)). The red disk galaxy population should be the result of transformations of the blue, late-type galaxies via mechanisms of gas depletion and consequently of SF quenching. The galaxy transition from star forming to quiescent, is highlighted by the presence of an intermediate zone, the so-called *green valley* (GV), on CMDs ([Martin et al., 2007](#); [Wyder et al., 2007](#); [Fang et al., 2012](#)). Investigating galaxies in the GV should shed light on the mechanisms governing the *on-off* state of the SF. S0s in groups, in particular, are key elements in identifying both the mechanisms and the environmental influence on their possible transformation.

Although S0s are early-type galaxies (ETGs), so they are widely considered evolved “red & dead” galaxies, *GALEX* (*Galaxy Evolution Explorer*) far-UV (FUV) and/or H α images revealed signatures of on-going star formation in their disks in the form of outer blue ring/arm-like structures in some of them. [Salim et al. \(2012\)](#), and references therein) show a wide collection of these kind of galaxies. Signatures of ongoing ($\approx 9_{-3}^{+4}\%$) or recent ($\approx 47_{-7}^{+8}\%$) SF are also found in the nuclear regions of nearby ETGs (e.g. [Rampazzo et al., 2013](#)).

The presence of a disk and the occurrence of SF in ETGs imply that cold gas has played an important role in their evolution. In [Figure 1](#) we show the optical (left panels) and UV colour composite images (middle panel) of examples of nearby S0s with outer ring/arm-like structures detected in the FUV band: NGC 404 ([Thilker et al., 2010](#)), NGC 1533, NGC 2962, NGC 2974 ([Marino et al., 2011a](#)), and NGC 1317 ([Gil de Paz et al., 2007](#)). All the S0s in [Figure 1](#) are located in low density environments. These galaxies also have cold gas, distributed either over the main body of the galaxy or forming large-scale structures around the galaxy, as shown by HI contours over plotted in the right panels of [Figure 1](#).

The paper explores the evolution of these S0s, using SPH simulations accounting for chemo-photometric evolution, i.e providing the SED at each evolutionary time (snapshot). The SED takes into account chemical evolution, stellar emission, internal extinction and re-emission by dust in a self-consistent way, as already described in MC03, [Spavone et al. \(2009\)](#), and references therein), and [Spavone et al. \(2012\)](#). The SED extends over four orders of magnitude in wavelength, i.e., from 0.1 to 1000 μm . Each simulation self-consistently provides morphological, dynamic and chemo-photometric evolution.

Simulations of groups, focusing on galaxy morphological transformation

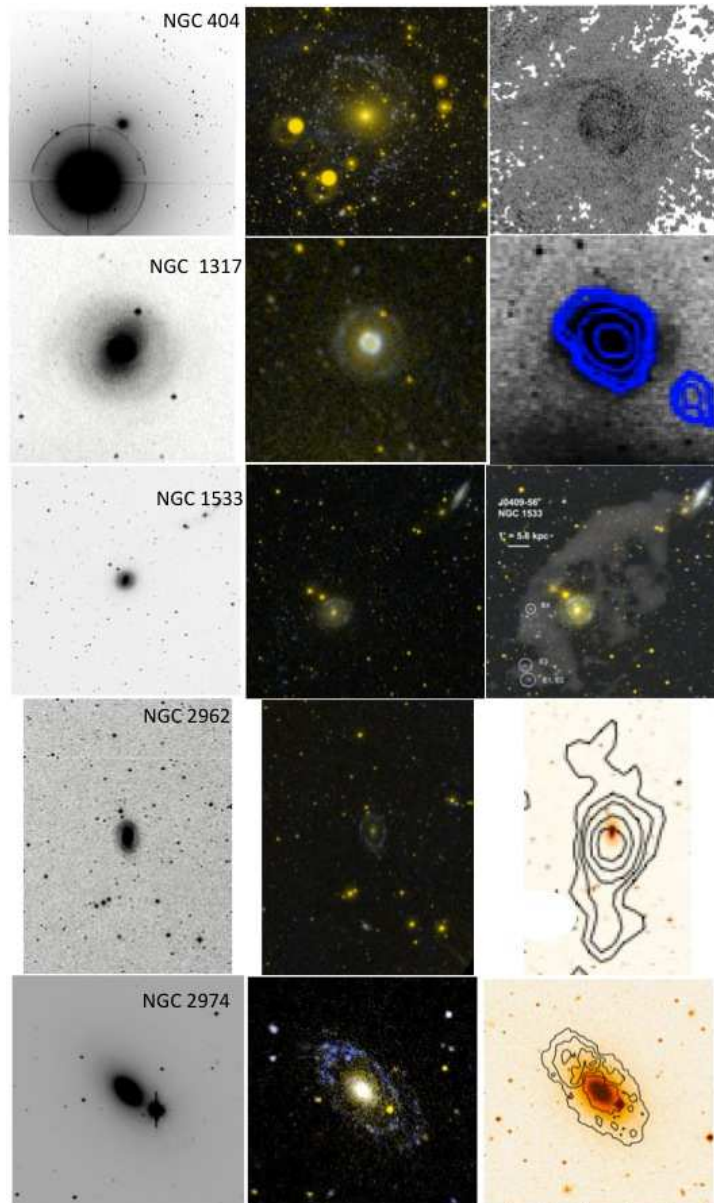


Figure 1: Composite view of five S0s with outer ring/arm-like structures detected in the FUV. From left to right: optical (left), UV two colours FUV (blue) and NUV (yellow) composite images (mid), and HI distribution or contours (right), are shown on the same scale. NGC 404 images are adapted from [Thilker et al. \(2010\)](#), NGC 1533, NGC 2962, and NGC 2974 from [Marino et al. \(2011a\)](#), NGC 1317 from [Gil de Paz et al. \(2007\)](#). HI images: NGC 1533 from [Werk et al. \(2010\)](#), NGC 1317 from [Horellou et al. \(2001\)](#), NGC 2962 from [Grossi et al. \(2009\)](#), and NGC 2974 from [Weijmans et al. \(2008\)](#).

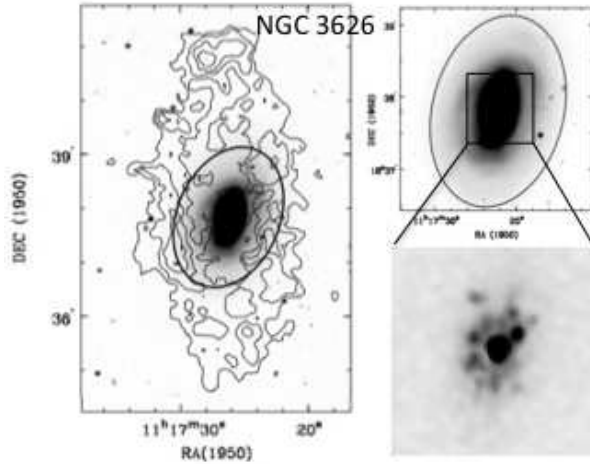


Figure 2: *Left:* Optical (R-band) image of NGC 3626 with HI contours superposed. *Right:* Optical (top) and H α (bottom) images adapted from Haynes et al. (2000). The ellipse has the dimension $D_{25} \times d_{25}$ and is oriented along the optical major axis of the galaxy; d_{25} is $1'.51$ (NED).

have been approached with different techniques (e.g. Kawata & Mulchaey (2008); Bekki & Couch (2011); Villalobos et al. (2012)). Kawata & Mulchaey (2008) used a cosmological chemo-dynamical simulation to study how the group environment affects the SF properties of a disk galaxy. Bekki & Couch (2011), starting from already formed galaxies, show that Sps in group environments can be strongly influenced by repetitive, slow encounters so that galaxies with thin discs can be transformed into thick discs, and gas poor S0s. Villalobos et al. (2012) perform 17 experiments in order to study the general evolution of disc galaxies, composed of a stellar disc embedded in a DM halo, within a group environment. This is modelled as an N-body DM halo following a Navarro et al. (1997) density profile including a spherically symmetric stellar component at its centre.

None of the quoted simulations explore the merger scenario combining the chemo-dynamical code with evolutionary population synthesis (EPS) models providing the galaxy SED at each evolutionary time (snapshot hereafter). This upgrade in galaxy simulations is the novelty of this paper.

As a case study we focus on simulations of two S0s with ring/arm like structures, detected in the far UV and/or narrow band optical images, im-

Table 1: Structural, photometric and kinematics properties of NGC 1533 and NGC 3626

Name	T	Dist [Mpc]	D_{25} [kpc]	r_e [kpc]	M_B [mag]	ΔV_{gas} [km s ⁻¹]
NGC 1533	SB0-	26.1 ± 1.9	10.3	1.6	-19.59 ± 0.38	132.1 ± 6.3
NGC 3626	(R)SA(rs)0+	11.0 ± 0.8	22.3	3.3	-20.11 ± 0.42	191.1 ± 5.3

merged in extended HI emission, namely NGC 1533 (Fig. 1) and NGC 3626 (Fig. 2). Both galaxies are members of groups (Marino et al., 2013, 2011b). NGC 3626, is located within the virial radius of USGC U376 (Ramella et al. (2002), Mazzei et al. 2013, in prep.) and NGC 1533 is a member of the Dorado group. They have extended SEDs, from FUV to far-IR (FIR), that we will use, together with their B-band absolute magnitude, to constrain our simulations. The detailed surface photometry and the 2D kinematical properties of the gas and stars of NGC 3626, also available from the literature, will be a further constraint.

The SPH simulations best-fitting their global properties are selected over a large grid of encounters from halos initially composed of DM and gas. In addition, our simulations highlight the evolutionary path through the GV in the CMD, of such galaxies.

The structure of the paper is as follows. Section 2 describes the observed properties of NGC 3626 and NGC 1533. Section 3 provides the details of our grid of SPH simulations. In Section 4 we compare the global measured galaxy properties with the results of our simulations. Section 5 discusses the galaxy evolution provided by the simulation focusing on the path of the near-UV(NUV)/optical colours in the ($NUV-r$) vs. M_r CMD. In Section 6 we draw our conclusions.

2. Photometric and kinematic properties of NGC 1533 and NGC 3626

The relevant properties of NGC 1533 and NGC 3626 are summarized in Table 1: columns 2 and 3 give the morphological type and the cosmological distance from NED¹; column 4 the apparent diameter corrected for galactic extinction and inclination, D_{25} , from HYPERLEDA², (Paturel et al., 2003);

¹NASA/IPAC Extragalactic Database <http://ned.ipac.caltech.edu>

²<http://leda.univ-lyon.fr>

column 5 the effective radius, r_e from the RC3 catalogue (de Vaucouleurs et al., 1991), column 6 the absolute B-band magnitude derived from the mean distance modulus computed from redshift-independent distance measurements (NED), and column 7 the maximum rotation velocity corrected for inclination from HYPERLEDA. D_{25} and r_e are reported in kpc using cosmology corrected scales from NED with cosmological parameters $H_0=70$ km/s/Mpc, $\Omega_{matter}=0.27$, $\Omega_{vacuum}=0.73$.

NGC 1533 is a SB0– in the RC3 catalogue (de Vaucouleurs et al., 1991), a SB02(2)/SBa in the RSA catalogue (Sandage & Tammann, 1987), and a $(L)SB(rs)0^0$ in the NED database. This latter classification implies a large lens outside the bar and an inner ring (Laurikainen et al., 2006). Marino et al. (2011a) found a prominent outer ring in the UV images extending from 39" to 80", and consisting of young (≤ 200 Myr old) stellar populations. More details on GALEX observations are given in Marino et al. (2011b). Werk et al. (2010) found a large-scale distribution of HI around the galaxy, as shown in Fig. 1. Ryan-Weber et al. (2003) reported HI arcs around the galaxy, spanning from 2' to 11'.7 outside the FUV ring, with a mass of $9.3 \times 10^8 M_\odot$ (their Table A1). They concluded that the HI is most likely the remnant of a tidally disrupted galaxy. This HI mass estimate increases by at least 6 times adopting the distance in DeGraaff et al. (2007). From optical spectroscopy in the central region of this galaxy, Annibali et al. (2007) derived an age of 11.9 ± 6.9 Gyr. DeGraaff et al. (2007) describes NGC 1533 as a galaxy which is completing a transition from late to early type: it is red, but not completely dead.

NGC 3626 is a lenticular galaxy with an outer (quite faint) ring (RLAT+..) in the RC3 catalogue (de Vaucouleurs et al., 1991), a normal Sa in the RSA catalogue (Sandage & Tammann, 1987) and a normal S0 galaxy in the NED classification (Table 1). It has inner and outer rings starting from an arm-like structure

Photometric (Sil'chenko et al., 2010; Afanesiev & Sil'chenko, 2007; Laurikainen et al., 2005) and kinematic observations (Ciri et al., 1995; García-Burillo et al., 1998; Haynes et al., 2000) show that its structure and kinematics are quite complex. Figure 2 illustrates its wide scale and inner properties. A wide dust-lane west of the nucleus is clearly visible within 1' (Haynes et al., 2000, their Fig. 5). Ionized gas and CO disks counter-rotate with respect to stars (Ciri et al., 1995; García-Burillo et al., 1998). The stellar vs. ionized gas velocity profiles are followed out to 45", i.e., $0.5 R_{25} \sim 6$ kpc, and 30"

respectively, on both sides of the galaxy (Haynes et al., 2000). HI VLA data (Haynes et al., 2000) show that the cold gas extends about 3' each side of the optical nucleus. The HI kinematics confirms the large-scale decoupling of the stars and gas. Evidence of an additional HI gas component co-rotating with the stars is suggested by (Haynes et al., 2000), as hinted also in the ^{12}CO map by García-Burillo et al. (1998). ^{12}CO emission is concentrated in a compact nuclear disk of average radius $r=12''$. From $R=20''$ to $R=100''$ ^{12}CO is not detected, and the neutral gas content is largely dominated by HI. The HI in the inner regions avoids the nucleus, where $\text{H}\alpha$ emission dominates, but follows closely the $\text{H}\alpha$ outside (Haynes et al., 2000).

Laurikainen et al. (2005), from a Fourier analysis of the K_s -band image of the galaxy, suggest the presence of a $40''$ long bar, and of an inner ($<5''$) elliptical structure, likely a secondary bar or a disk structure with a twisted (10°) position angle with respect to the main disk. Sil'chenko et al. (2010) find indications of two stellar disks. The inner disk extends from $10''$ to $45''$ with a scale length of $19''.8 \pm 0''.7$ (*i* SDSS band), and the outer one has a scale length of $21'' \pm 2''$. The bulge is very compact with an effective radius of $2''.52 \pm 0''.05$. Sil'chenko et al. (2010) derived an age younger than 2 Gyr in the central part of NGC 3626, suggesting the occurrence of a recent accretion episode.

The calibration of Bell (2003) and Hopkins et al. (2003) allows us to derive the star formation rate (SFR) from the radio flux (1.4 GHz). Adopting a luminosity distance of 26.1 Mpc and the measure of Condon et al. (2002) at 1.4 GHz, the SFR of stars more massive than $5 M_\odot$ is $\simeq 1.7 M_\odot/\text{yr}$. This becomes $0.5 M_\odot/\text{yr}$ using Cram et al. (1998) calibration.

3. The grid of SPH chemo-photometric simulations

Our SPH simulations of galaxy formation and evolution start from the same initial conditions as described in Mazzei & Curir (2003, MC03 hereafter) and Curir & Mazzei (1999) i.e. a collapsing triaxial systems initially composed of dark matter (DM) and gas in different proportions and different total masses. In more detail, each system is built up with a spin parameter, λ , given by $|\mathbf{J}||E|^{0.5}/(GM^{0.5})$, where E is the total energy, J the total angular momentum and G the gravitational constant; λ is equal to 0.06 and aligned with the shorter principal axis of the DM halo. The triaxiality ratio of the DM halo, $\tau = (a^2 - b^2)/(a^2 - c^2)$, where $a > b > c$, is 0.84 (Warren et al., 1992).

All the simulations include self-gravity of gas, stars and DM, radiative cooling, hydrodynamical pressure, shock heating, artificial viscosity, star formation (SF), feedback from evolved stars and type II SNe, and chemical enrichment as in MC03 (and references therein). *They provide the synthetic SED at each evolutionary step, i.e., at each snapshot, accounting for evolutionary population synthesis models.* The SED takes into account chemical evolution, stellar emission, internal extinction and re-emission by dust in a self-consistent way, as described in previous works (Spavone et al. (2009) and Spavone et al. (2012, and references therein)). This extends over four orders of magnitude in wavelength, i.e., from 0.1 to 1000 μm . Each simulation self-consistently provides morphological, dynamic and chemo-photometric evolution. The Initial Mass Function (IMF) is of Salpeter type with upper mass limit $100 M_{\odot}$ and lower mass limit $0.01 M_{\odot}$ (Salpeter, 1955) as in Curir & Mazzei (1999) and MC03. All the model parameters adopted here had been tuned in previous papers where the integrated properties of simulated galaxies, i.e., colours, absolute magnitudes, mass to luminosity ratios provided by different choices of model parameters after 15 Gyr, had been successfully compared with those of local galaxies (see also Mazzei (2003); Mazzei (2004)). In particular, from this IMF choice a slightly higher SFR arises compared with the other possibilities examined; this allows for the lowest feedback strength, and for the expected rotational support when disk galaxies are formed (Curir & Mazzei, 1999; Mazzei & Curir, 2003). Moreover, as pointed out by Kroupa (2012), its slope is almost the same as the Universal Mass Function which links the IMF of galaxies and stars to those of brown dwarfs, planets and small bodies (meteoroids, asteroids) (Binggeli & Hascher, 2007).

With respect to MC03, the particle resolution is enhanced here to $4\text{-}8 \times 10^4$ instead of $1\text{-}2 \times 10^4$, so there are $2\text{-}4 \times 10^4$ particles of gas and $2\text{-}4 \times 10^4$ of DM at the beginning in each new simulation. Moreover the time separation between the snapshots has been halved; it is now 37 Myr. The gravitational softenings are 1, 0.5, and 0.05 kpc respectively for DM, gas, and star particles.

A new large set of galaxy encounters involving systems with 1:1 and different mass ratios have been performed with the same initial conditions as described in MC03. By seeking to exploit a wide range of orbital parameters, we carried out different simulations for each couple of interacting systems varying the orbital initial conditions in order to have, for the ideal Keplerian orbit of two points of given masses, the first peri-center separation, p , equal to the initial length of the major axis of the more massive triaxial halo down to 1/10 of the same axis. For each peri-center separation we changed the

eccentricity in order to have hyperbolic orbits of different energy. The spins of the systems are generally parallel each other and perpendicular to the orbital plane, so we studied direct encounters. Some cases with misaligned spins have been also analysed in order to investigate the effects of the system initial rotation on the results. For a given set of encounters with the same orbital parameters we also examined the role of increasing initial gas fractions.

4. Comparing data with models

From the grid of physically motivated SPH simulations, we isolate those simultaneously best-fitting the global properties, i.e., the total SED, the B-band absolute magnitude, and the photometric and kinematics properties of NGC 1533 and NGC 3626, presented in § 2. The selected snapshot corresponds to the best-fit age of the galaxy, given in the following.

We find that both the galaxies are well matched by *the same simulation at different evolutionary times*.

The simulation consists of a merger of two triaxial collapsing systems initially composed of DM and gas with mass ratio 2:1 and total mass $3.0 \times 10^{12} M_{\odot}$. The starting point corresponds to 6×10^4 particles, 3×10^4 of gas and 3×10^4 of DM with a relative mass gas ratio of 0.1. The gas mass resolution is $10^7 M_{\odot}$, that of the DM particles ≈ 9 times larger. The spins of the systems are equal ($\lambda=0.06$, MC03), perpendicular, and both aligned with the shorter of their principal axes. The initial parameters of the encounter are reported in Table 2. In particular the first peri-centre separation, p , corresponds to 1/10 of the major axis of the principal system, the orbit eccentricity is 1.3, and the anomaly corresponds to 200° . The variables r_1, r_2, v_1, v_2 in Table 2 are the initial positions and velocities with respect to the centre of mass of the system of the two halos having masses M_1 and M_2 .

In the following, we discuss in detail the comparison of our models with the available data for the two galaxies discussed in §2.

4.1. NGC 3626

The galaxy age is of 11.5 Gyr. The average stellar age within the effective radius, r_e provided in Table 1, is 4.3 Gyr and increases to 5.5 Gyr within $R_{25} \simeq 3 r_e$. These age estimates become younger if stellar ages are weighted by the B-band luminosity: 3.4 Gyr and 4.5 Gyr respectively. In the inner

Table 2: Input parameters of SPH simulation of NGC 3626 and NGC 1533

p	R_1 [kpc]	R_2 [kpc]	v_1 [km s ⁻¹]	v_2 [km s ⁻¹]	M_1 [10 ¹⁰ M_\odot]	M_2 [10 ¹⁰ M_\odot]	f_{gas}
101	273	546	52	104	200	100	0.1

regions, $R \leq 1.5$ kpc, stars are younger than 2 Gyr, in good agreement with the findings of [Sil'chenko et al. \(2010\)](#).

The SFR, i.e. the mass of stars younger than 0.01 Gyr, is $2 M_\odot/\text{yr}$, in agreement with the radio estimates given by [Bell \(2003\)](#) (see §2).

4.1.1. Photometric properties

Figure 3 compares the J-band image of NGC 3626 (top left panel) with the XZ projection (top right panel) of the selected snapshot in the same band with the same spatial scale. Our simulation well reproduces the observed morphology.

The absolute B-band magnitude of the model, $M_B = -20.23$, agrees with the observed value reported in Table 1.

The entire SED is also well matched by our simulation at the selected snapshot (Fig. 3, left bottom panel). The SED refers to the total fluxes of the galaxy and extends from FUV to $160 \mu\text{m}$, i.e. over almost three orders of magnitude in wavelength. UV band data are from [Rifatto et al. \(1995\)](#) and FIR data, at 65, 90, 140, and to $160 \mu\text{m}$ ³, from AKARI/FIS Bright Source Catalog ([Yamamura et al., 2009](#)). The predicted SED in the FIR is composed of a warm and a cold dust component and includes PAH molecules as discussed in [Mazzei et al. \(1992\)](#). Warm dust is located in regions of high radiation field, i.e., in the neighbourhood of OB clusters, whereas cold dust is heated by the general interstellar radiation field. The distribution of diffuse radiation is the same as in the Milky Way ([Mazzei et al., 1992](#)), however its intensity, $I_0 = 30 I_{local}$, is almost four times higher than in normal spirals. Therefore, the temperature distribution of the cold dust component peaks at almost 25K instead of 20K as in the Milky Way. The warm dust temperature is not well constrained since no data are available in the 20-60 μm spectral range. Our fit corresponds to a warm dust temperature of ~ 55 K and to a warm-to-cold energy ratio of 0.23, as in [Mazzei et al. \(1992\)](#). Therefore,

³65 and $160 \mu\text{m}$ are upper limits

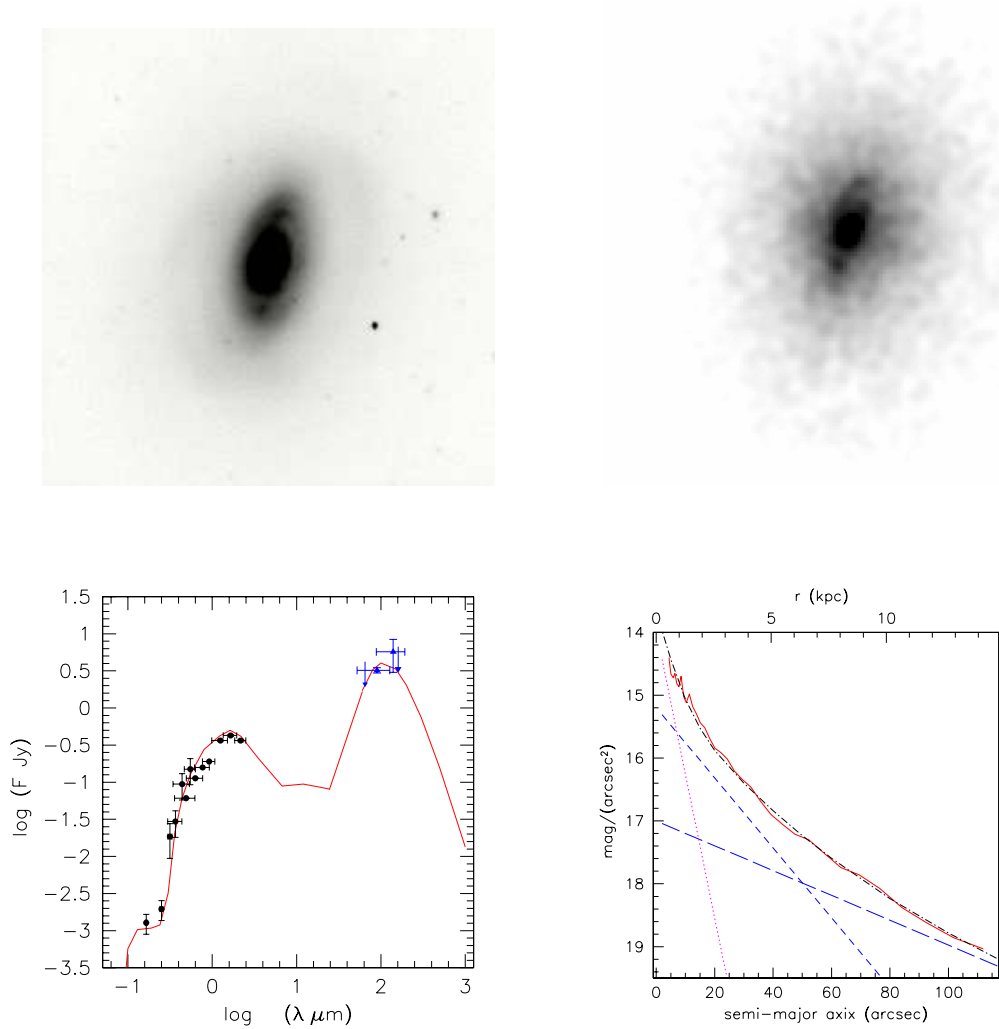


Figure 3: *Top*: $2.9' \times 2.9'$ J-band image of NGC 3626 (left), and simulated J-band map (right) on the same scale (resolution is $2''/\text{px}$). *Bottom left*: Red solid line shows the prediction of our model for NGC 3626, filled circles are data from FUV to NIR spectral range NED, (blue) triangles in the FIR are from the AKARI/FIS Bright Source Catalog (Yamamura et al., 2009); error bars account for band width and flux 3σ uncertainties. *Bottom right*: J-band brightness profile (red solid line) of our simulated map and its best-fit (dot-dashed line); dotted line shows the bulge distribution using a de Vaucouleurs law with $R_e=8''$ and $\mu_J(0)=15.8 \text{ mag/arcsec}^2$; short-dashed line: the inner disk with scale length $19.5''$ and $\mu_J(0)=15.2 \text{ mag/arcsec}^2$; long-dashed line: the outer disk with $55''$ and 17 mag/arcsec^2 .

the FIR SED is accounted for by the diffuse radiation of disk stars on dust grains since cold dust provides about 80% of the FIR emission. This is not surprising given the small bulge characterizing this S0 system: its bulge-to-total light ratio is 0.25 (Laurikainen et al., 2005). The fraction of bolometric luminosity of such a galaxy in the FIR is 34%, similar to that expected for Spirals and at least 10 times higher than the average of S0 galaxies (Mazzei & De Zotti, 1994).

We derive the J band luminosity profile of our simulated image (Fig. 3 right, bottom panel) using the ELLIPSE package (Jedrzejewski, 1987) in IRAF. To perform the best-fit of the surface brightness profile, we follow the strategy adopted by Sil'chenko et al. (2010) using SDSS images (Sect. §2.). We derive the inner disk extending from 7" to 50" with scale length 19".5, in good agreement with the cited paper, and the outer disk, beyond 50", with larger scale length, 55". This is possible since our model is not background limited. The central region is well matched by a de Vaucouleurs law, typical of a bulge (Fig. 3). We point out that the J central surface brightness of our outer disk is 17 mag/arcsec². This becomes 20.7 mag/arcsec² in the B-band accounting for the intrinsic total colour, (B-J)≈3 mag, and the average total B-band internal reddening, 0.7 mag (derived from our SED). This value is well within the range assumed by the extrapolated central surface brightness of spiral disks (see Phillipps & Disney, 1983).

All the photometric properties analysed, are well matched at the selected snapshot of our simulation.

4.1.2. Kinematics

Figure 4 (left panel) shows the distribution of the different mass components within 33 kpc, i.e., ≈10 r_e , at the selected snapshot. There is a large amount of gas inside this radius, $8.5 \times 10^9 M_\odot$. All this gas has a temperature lower than 2×10^4 K. Since the cooling time of the gas is much shorter than the snapshot time range (0.037 Gyr), this amount represents the upper limit of the mass of the coldest gas within the radius considered. In particular, the mass of gas with temperature $T \leq 10^4$ K, which marks more closely the regions of SF, is $2 \times 10^9 M_\odot$, in good agreement with the value of $1.1 \times 10^9 M_\odot$ given by Haynes et al. (2000, their Table 8).

Fig. 4 (right panel), shows the same XZ projection as in Fig. 3 with gas contours overlaid. The disk of gas appears edge-on, rotating along the X-axis, coplanar with the stars.

The rotation curve of the cold gas (i.e. $T \leq 10^4$ K), is compared with the

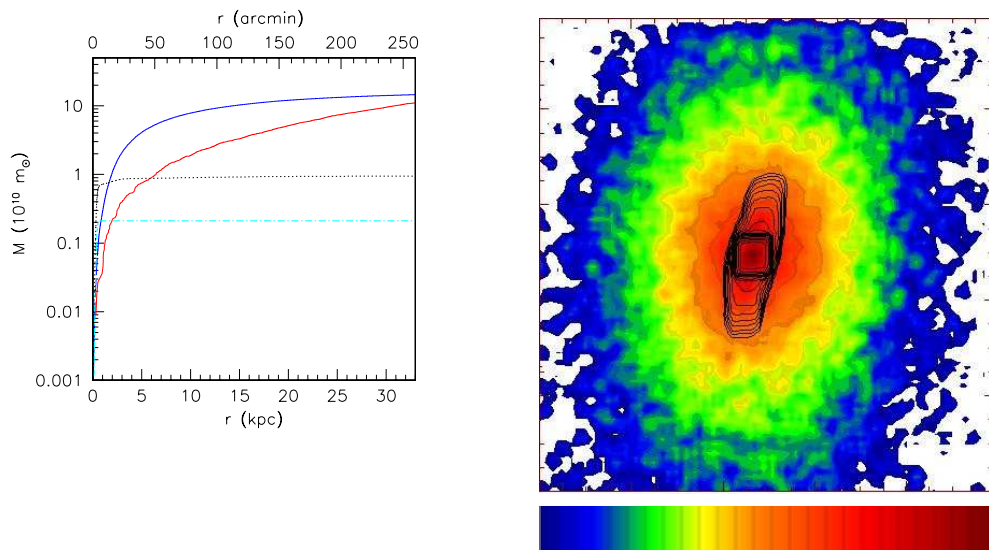


Figure 4: *Left*: Mass distribution inside a radius of $33 \text{ kpc} \simeq 10 r_e$ centered on the V-band galaxy centre: (red) solid line shows the DM mass, (blue) long-short dashed line stars, (black) dotted line gas, and (cyan) dot-dashed line cold gas ($T < 10^4 \text{ K}$). *Right*: $2'.9 \times 2'.9$ XZ projection in the J-band of the selected snapshot. The map has been normalized to the total flux and includes 60 equally spaced levels spanning a contrast of 200; in the colour scale, blue corresponds to the lower and red to the higher density contrast. Twenty equally spaced levels showing the morphology of the cold gas are over plotted on the star contours.

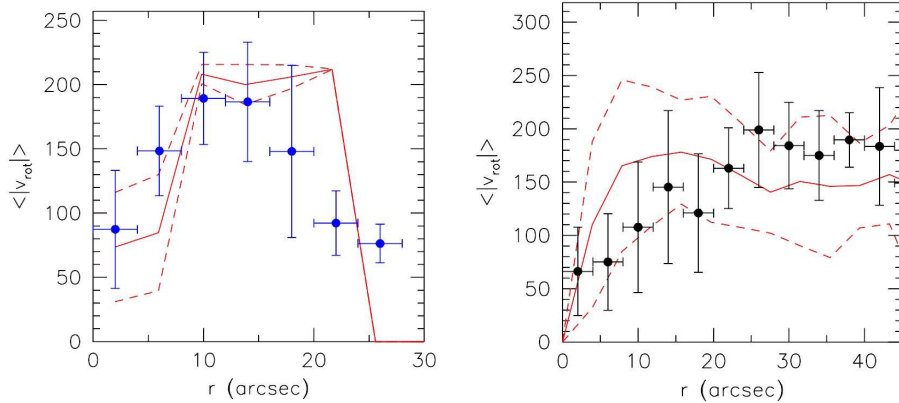


Figure 5: Rotation curve of gas (left) and stars (right) compared with our predictions. Filled circles, binned within $4''$, indicate gas measurements (left) by Ciri et al. (1995); Haynes et al. (2000) and star data (right) by (Haynes et al., 2000); vertical bars show the velocity dispersion of observations within each bin. Dashed lines indicate the velocity dispersion of our snapshot, showing the range of model predictions.

observations of Ciri et al. (1995) and Haynes et al. (2000, P.A. 157 degrees) in Fig. 5 (left panel). Both the data and the snapshot velocities are binned to a spatial resolution of $4''$. We emphasize that increasing the gas temperature limit to 2×10^4 K, the rotation curve rises to 25 kpc, in agreement with the large disk, extending well beyond the optical radius of the galaxy (i.e., $2.6 \times D_{25}$), detected by Haynes et al. (2000). Figure 5 (right panel) compares the stellar velocity curve of our simulation, at the selected snapshot, with observations (Ciri et al., 1995; Haynes et al., 2000).

Both the rotation curves well reproduce the observed ones within the errors.

4.2. NGC 1533

The same simulation which best fits the global properties of NGC 3626, also matches those of NGC 1533 at a snapshot 2.15 Gyr older. This corresponds to a galaxy age of 13.7 Gyr. The average stellar age within the effective radius, r_e (Table 1), is 6.5 Gyr and within $R_{25} (\simeq 3 r_e)$, is 7 Gyr. These estimates become younger if the stellar age is weighted by the B-band luminosity: 3.7 Gyr and 6 Gyr respectively. The B-band absolute magnitude, $M_B = -19.89$ mag, agrees with the observed value reported in Table 1.

The SFR, i.e. the mass of stars younger than 0.01 Gyr, is $0.14 M_{\odot}/\text{yr}$, and the total SFR, i.e., the total mass of stars born within the snapshot time-step, is $0.26 M_{\odot}/\text{yr}$.

4.2.1. Photometric properties

Figure 6 (top panels) compares, on the same scale, the observed composite FUV and NUV image (left) with the selected snapshot (right). Figure 6 (bottom left panel) presents both the observed SED of NGC 1533 and the best-fit obtained from the selected simulation. The SED refers to the total flux of the galaxy. FUV and NUV total magnitudes are derived from Table 3 of Marino et al. (2011b) and corrected for foreground galactic extinction following prescriptions in NED (Fitzpatrick, 1999).

The entire SED is well matched at the selected snapshot. The predicted FIR SED is composed of warm and cold dusts as discussed in Sect §4.1.1. The intensity of the diffuse radiation field, $I_0=7I_{local}$, is the same as in the Milky Way (Mazzei et al., 1992). The warm dust temperature is well constrained by MIPS data of Temi et al. (2009a) at 24 and $70 \mu\text{m}$. Our fit provides a warm dust temperature of 52 K and a warm-to-cold energy ratio 0.15. Therefore, also in this case, the SED in the FIR is accounted for by the diffuse radiation field of disk stars on dust grains since cold dust accounts for 85% of FIR emission. As for NGC 3626, a small bulge characterizes this S0; its bulge-to-total light ratio is 0.25 (Laurikainen et al., 2006). The fraction of bolometric luminosity which comes out in the FIR, 10%, is 3 times less than that expected for Sps but five times more than the average for S0s (Mazzei & De Zotti, 1994; Mazzei et al., 1994).

The total mass of the galaxy inside D_{25} is $4.9 \times 10^{10} M_{\odot}$ with a DM fraction of 0.17, and a mass-to-light ratio in the B-band of $25.8 M_{\odot}/L_{\odot}$.

Figure 6 (bottom right panel) shows the distribution of the different mass components at the selected snapshot within 16 kpc, i.e., $\simeq 10 r_e$. The mass of cold gas, $1.0 \times 10^9 M_{\odot}$, is in good agreement with the findings by Ryan-Weber et al. (2003), given in Sect. §2.

5. Insights into the evolution of NGC 3626 and NGC 1533

5.1. The (NUV- r) vs. Mr CMD

As discussed by Schawinski et al. (2007), (NUV- r) colour is an excellent tracer of even small amounts ($\simeq 1\%$ mass fraction) of recent (≤ 1 Gyr) star formation. In this context, the (NUV- r) CMD has been used to study the

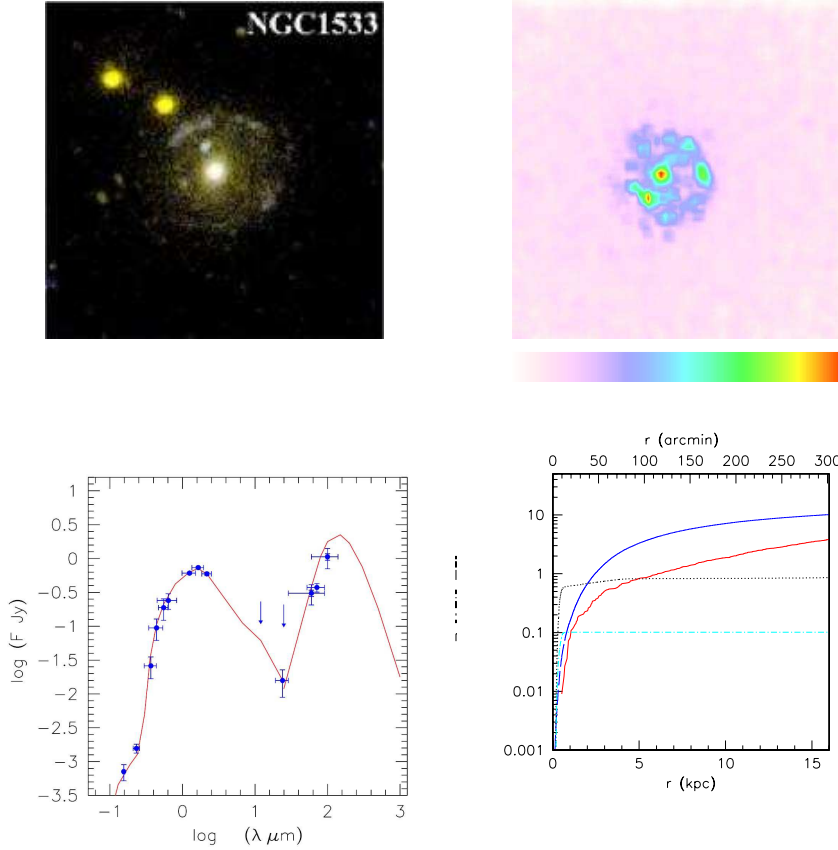


Figure 6: *Top*: $5' \times 5'$ colour composite UV (FUV blue, NUV yellow) image of NGC 1533 (left) and the simulated YZ projection FUV/NUV map (right), on the same scale. Flux has been normalized to the total flux. The map includes 60 equally spaced levels with a density contrast of 20. *Bottom*: FUV to far-IR SED of NGC 1533 (left); blue points are the measured total fluxes from *NED*; error bars account for band width and 3σ uncertainties of the flux; red line is the prediction of our model. *Bottom right*: Mass distribution inside a radius of $16 \text{ kpc} \simeq 10 r_e$ centered on the V-band galaxy centre (right); symbols are as in the left panel of Fig. 4.

effect of environment on the recent star formation history in large sets of galaxies observed with *GALEX* (Salim et al., 2005).

Our approach allows us to understand how the galaxy transforms, i.e. what is its evolutionary path in this diagram (Fig. 7).

The simulated galaxy gets to the blue sequence (Wyder et al., 2007) after 0.4 Gyr from the beginning, and follows it for 7.2 Gyr, when reaching its maximum SFR (Fig. 8, left) and, correspondingly, its brighter $M_r(\text{AB})$ magnitude. At this point of the evolution, only 12% of the galaxy bolometric luminosity is absorbed and re-emitted in the FIR and the galaxy is about 2 magnitudes brighter in the B-band than at the age of our best-fit for NGC 3626, i.e., 11.5 Gyr.

Figure 8 (left) shows that the total SFR fades as the gas fueling decreases (right). Moreover, its active phase lasts 7.2 Gyr, then the SFR turns off within 1 Gyr. Correspondingly, as shown in Fig. 7, the galaxy leaves the blue sequence within 1 Gyr. Then it crosses the GV to achieve the current position of NGC 3626 in 3.4 Gyr, and stays in the red sequence up to the end of our simulation (≈ 14 Gyr).

The effect of dust attenuation, i.e. the internal reddening, evaluated accounting for an inclination angle of $\sim 60^\circ$ (i.e. 56° for NGC 3626, and 64° for NGC 1533 (HYPERLEDA), does not modify this picture. The attenuation, indeed, is quite negligible until the galaxy is 7 Gyr old, due to the active role of the SFR (Fig. 8, left) which reduces the cold gas (Fig. 8, right). The internal reddening rises to $A_{(NUV-r)}=0.13$ mag and $A_r=0.07$ mag at 8.1 Gyr, it increases to 0.52 and 0.30 mag respectively at 11.5 Gyr, the age of NGC 3626, and reduces to 0.24 and 0.13 mag at 13.7 Gyr, the age of NGC 1533. The reddening is quite negligible at 14 Gyr, the last point in Fig. 7. This finding agrees with the value of attenuation for ETGs (Salim et al., 2005), i.e. their attenuation decreases as their (NUV- r) colour becomes redder. Moreover, the amount of reddening we predict in the GV and red-sequence regions of the CMD, agrees, within the errors, with the average value estimated by Martin et al. (2007, and references therein) even if Martin et al. (2007) used the Calzetti et al. (1994) law, whereas we adopt our own Galaxy extinction law (Mazzei et al., 1992).

The simulation here does not predict strong oscillations in the GV, however different evolutionary paths in such a CMD are possible for early-type galaxies, as will be discussed in a forthcoming paper (Mazzei et al. 2013, in prep).

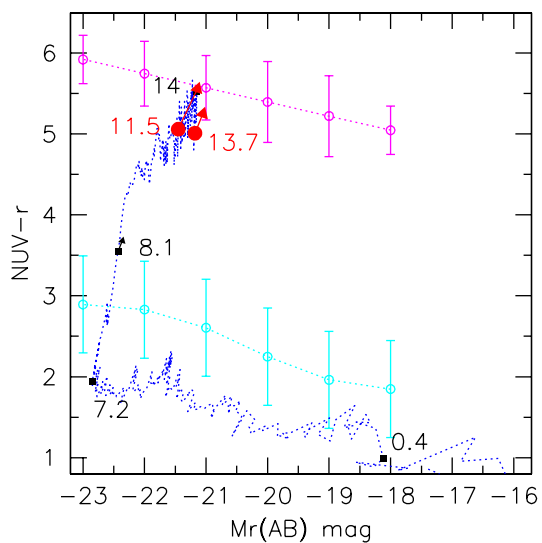


Figure 7: The $(\text{NUV}-r)$ vs M_r CMD of our simulation best-fitting the global properties of NGC 3626 and NGC 1533. Dotted line shows its evolutionary path; filled squares mark some meaningful evolutionary times in Gyr;(red) filled circles show the current position of NGC 3626 and NGC 1533; arrows emphasize the reddening effect. The Wyder et al. (2007) fits of the blue (cyan) and red (magenta) sequences are plotted including their error bars.

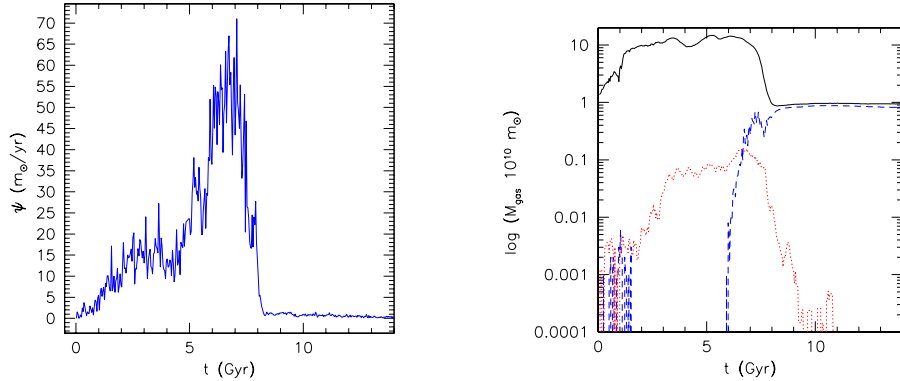


Figure 8: *Left:* The time-evolution of the total SFR. *Right:* (black) solid line shows the evolution of the gas mass inside a radius of 50 kpc centered on the V-band luminous centre of the galaxy; (blue) dashed line corresponds to the gas with temperature $\leq 2 \times 10^4$ K, and the (red) dotted line to the gas with temperature $\geq 10^6$ K.

5.2. Photometric evolution

Figure 9 compares, at three meaningful evolutionary ages, the isophotal J-band brightness profiles (XZ projections) of the corresponding snapshots, position angles and ellipticities as derived from simulated maps with the same resolution as that in Fig. 3 (top right panel) and Fig. 4 (right panel). Taking into account that our approach aims to reproduce the global properties of the galaxy, not all the details, Figure 9 shows that a disk profile characterizes the galaxy morphology at 7 Gyr, when the galaxy is located on the blue sequence of the CMD (Fig. 7). Therefore, accounting for results in Sect. §4.1.1, a bulge progressively appears, and an outer disk is maintained during the evolution, i.e., along the GV up to the red sequence. The position angle of the isophotes changes with time, although it does not show any significant twisting.

Table 3 summarizes galaxy predictions inside a region of 11 kpc, corresponding to the R_{25} radius of NGC 3626, as a function of the ages reported in column 1. We point out that the r_e of NGC 3626, as well as its R_{25} , are about twice those of NGC 1533 (Table 1). The galaxy properties reported in Table 3 are: the average age of the stellar populations weighted by the B-band luminosity, t_{gen} (column 2), the total mass (column 3), the mass-

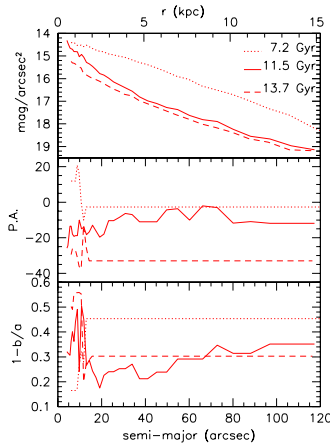


Figure 9: *Top*: compares the J-band brightness profiles of our simulation at 7.2 Gyr, when the galaxy leaves the blue sequence (dotted line), at 11.5 Gyr (solid line), i.e. the best-fit age of NGC 3626, and at 13.7 Gyr, the best-fit age of NGC 1533. All the profiles are derived from the XZ projection of the corresponding snapshot with the same resolution as in Fig. 3 (top right) and Fig. 4 (right). *Middle*: evolution of the position angle; symbols are the same as in the top panel. *Bottom*: evolution of the ellipticity.

Table 3: Results within 11 kpc

galaxy age Gyr	t_{gen} Gyr	M_{tot} $10^{10} M_{\odot}$	M/L_B M_{\odot}/L_{\odot}	f_{gas}	f_{DM}
7.2	0.6	11.0	2.3	0.22	0.19
11.5	4.5	11.5	18.8	0.08	0.19
13.7	7.0	10.5	33.2	0.08	0.19

t_{gen} : the average age of stellar population weighted on B-band luminosity

to-light ratio (column 4), the gas and DM mass fractions (column 5 and 6 respectively).

Table 3 provides the following picture. Inside the radius considered, the DM is a low, constant fraction of the total mass, corresponding to less than 20%, during all the evolution. The gas fraction decreases at the age of the best-fit of NGC 3626, then remains constant. It shows that the gas accretion rate and the SFR balance themselves within the radius considered. The mass-to-light-ratio increases with age following the decrease of the galaxy luminosity in the B-band.

6. Discussion and Conclusions

We are exploring the co-evolution of galaxies in groups combining multi wavelength photometric and 2D kinematical observations (Marino et al., 2013). S0s in groups are of particular interest since the possible transformation Sp→S0 may be tested in an environment physically different from that of a cluster. We simulate the evolution of Sa/S0 galaxies showing SF in ring/arm like structures both detected by H α and/or FUV observations and characterized by the presence of large-scale HI structures in and/or around them.

These ETGs are not so uncommon in low density environments, like groups. Serra & Oosterloo (2010) found that $\geq 25\%$ of ETGs contain HI at the level of $M(\text{HI}) \geq 10^8 M_{\odot}$, i.e. that $M(\text{HI})$ is of the order of a few per cent of the total stellar mass. Their HI interferometric observations revealed very disturbed gas morphology/kinematics in a vast majority of the detected systems, confirming the continuing assembly of many ETGs but also showing that these are not necessarily gas free. They also find that all very disturbed ETGs have a single-stellar-population-equivalent age < 4 Gyr.

Here we focus on two of such galaxies, NGC 3626 and NGC 1533. Our SPH simulations allow us to derive dynamical and morphological information as well as the SED extending over four orders of magnitude at each evolutionary stage.

We find that the global properties of both NGC 1533 and NGC 3626 are well matched by the same simulation, suggesting that their complex properties may be explained in the framework of galaxy encounters. In the specific case the driver of both the photometric and kinematics peculiarities of NGC 3626 and NGC 1533 is a major merging episode. The merger occurs from haloes initially composed of DM and gas with mass ratio 2:1, total mass $3 \times 10^{12} M_{\odot}$, and gas fraction 0.1. Star forming ring/arm like structures observed in the galaxy disk are features arising in the latter stages of the merger episode which starts after 3.5 Gyr from the onset of the SF. These features arise when the galaxy is almost 8 Gyr old, following the head-on collision driving the evolution of our systems (Moiseev & Bizyaev, 2009). NGC 3626 is 11.5 Gyr old, and NGC 1533 13.7 Gyr old. Their FIR SED is dominated by the emission of cold dust, heated by the diffuse radiation field which represents, in both the cases, at least 80% of the total FIR emission. Moreover, the fraction of bolometric luminosity which comes out in the FIR spectral range is five times and ten times larger for NGC 1533 and NGC 3626 respec-

tively, than the average for S0 galaxies (Mazzei & De Zotti, 1994). Using new AKARI/FIS catalogue data (Yamamura et al., 2009), we conclude that NGC 3626 is characterized by almost the same FIR fraction as the Milky Way, i.e. 30% (Mazzei et al., 1992).

Our chemo-photometric SPH simulations, including evolutionary population synthesis models, allow us to trace, in a fully consistent way, the evolutionary path of NGC 3626 and NGC 1533 in the $(NUV-r) - M_r$ CMD. The transition from the blue sequence, along which these galaxies evolved for about 7-8 Gyr, across the GV and before they became mature and red ETGs, lasts about 4-5 Gyr. Fasano et al. (2000) noticed that a sort of morphological conversion in the cluster galaxy population from Sp→S0 took place about 1 - 4 Gyr ago. This estimate agrees with the time scales of our simulations. Excursions into the GV from the red sequence, driven by the acquisition of fresh gas for star formation (Thilker et al., 2010), are not expected in the evolutionary picture characterizing these two galaxies, but are possible along different evolutionary paths (Mazzei et al. 2013, in prep). The global properties found for NGC 1533 and NGC 3626 arise from the same evolutionary framework already explored in Bettoni et al. (2012): a merging episode with a gas rich companion.

Several mechanisms have been proposed to explore transformation of Sp→S0 in groups, from *strangulation* (Kawata & Mulchaey, 2008), to repetitive slow encounters (Bekki & Couch, 2011) both grabbing gas from Sp, quenching star formation and suppressing arms. Our results show that another mechanism of gravitational origin, the merging of two haloes, is a *viable* mechanism to generate S0s today found in the red sequence, in agreement with suggestions by Boselli & Gavazzi (2006) and George et al. (2013).

Acknowledgments

We thank Martha Haynes for kindly sending us the H α image of NGC 3626 and Marcel Clemens for help in revising the text. RR, AM and DB acknowledge the partial financial support by contract ASI-INAF I/009/10/0. DB and RR acknowledge the partial financial support by contract INAF/PRIN 2011 “Galaxy Evolution with the VLT Survey Telescope (VST)”. This research has made use of the NASA/IPAC Extragalactic Database (NED) which is operated by the Jet Propulsion Laboratory, California Institute of Technology, under contract with the National Aeronautics and Space Administration.

We acknowledge the usage of the HyperLeda database (<http://leda.univ-lyon1.fr>).

References

- Afanesiev, V., Silchenko, O., *Leo II Group: decoupled cores of NGC 3607 and NGC 3608*, A&AT, 26, 311-337, 2007
- Annibali, F., Bressan, A., Rampazzo, R. et al., *Nearby early-type galaxies with ionized gas III. Analysis of line-strength indices with new stellar population models*, A&A, 463, 455-479, 2010
- Baldry I. K., Glazebrook, K., Brinkmann, J., Ivezić, Ž., Lupton, R. H., Nichol, R. C., & Szalay, A. S., *Quantifying the Bimodal Color-Magnitude Distribution of Galaxies*, ApJ, 600, 681-694, 2004
- Bekki, K. *Ram-pressure stripping of halo gas in disc galaxies: implications for galactic star formation in different environments*, MNRAS, 339, 2221-2230, 2009
- Bell, E.F., *Estimating star formation rates from infrared and radio luminosities: the origin of the radio-infrared correlation*, ApJ, 586, 794-813, 2003.
- Bekki, K, Couch, W. *Transformation from spirals into S0s with bulge growth in groups galaxies*, MNRAS, 415, 1783-1796, 2011
- Bettoni, D., Buson, L., Mazzei, P., Galletta, G., *Insight into the evolution of the innermost region of the NGC 1023 Group*, MNRAS, 423, 2957-2965, 2012
- Binggeli, B. & Hascher, T., *Is There a Universal Mass Function?*, PASP, 119, 592-604, 2007
- Boselli, A, Gavazzi G. *Environmental effects on late-type galaxies in nearby clusters*, PASP, 118, 517-559, 2006
- Calzetti, D., Kinney, A. & Storchi-Bergmann, T. *Dust extinction of the stellar continua in starburst galaxies: The ultraviolet and optical extinction law*, ApJ, 429, 582-601, 1994
- Ciri, R., Bettoni, D., Galletta, G., *A massive counter-rotating gas disk in a spiral galaxy*, Nature, 375, 661-663, 1995

- Condon, J., Cotton, W., Broderick, J., *Radio Sources and Star Formation in the Local Universe*, AJ, 164, 675-689, 2002
- Evolutionary path to and from the red sequence: star formation and HI properties of transition galaxies at $z \sim 0$* , MNRAS, 400, 1225-1240, 2009
- Cram, L., Hopkins, A., Mobasher, B., Rowan-Robinson, M., *Star Formation Rates in Faint Radio Galaxies*, ApJ, 507, 155-160, 1998
- Curir, A., Mazzei, P. *SPH simulations of galaxy evolution including chemophotometric predictions*, New Astron., 4, 1-20, 1999
- Dekel, A., Birnboim, Y. *Gas bimodality due to cold flows and shock heating*, MNRAS, 368, 2-20, 2006
- de Vaucouleurs, G., de Vaucouleurs, A., Corwin, H. G., Buta, R. J., Paturel, G., Fouque, P., *Third Reference Catalogue of Bright Galaxies*, 1991 (New York : Springer) (RC3)
- DeGraaff, R., Blakeslee, J., Meurer, J. *A galaxy in transition: structure, globular clusters, and distance of the star-forming S0 galaxy NGC 1533 in Dorado*, ApJ, 671, 1624-1639, 2007
- Fang, J.J., Faber, S.M., Salim, S., Graves, G.J., Rich, R.M., *The slow death (or rebirth?) of extended star formation in $z=0.1$ green valley early-type galaxies*, ApJ, 676, 23-39, 2012
- Fasano, G., Poggianti, B., Couch, W., Bettoni, D., Kjaergaard, P., Moles, M., *The Evolution of the Galactic Morphological Types in Clusters*, ApJ, 542, 673-683, 2000
- Freeman, K. C., *On the disks of Spiral and S0 galaxies*, ApJ, 160, 811-830, 1970
- Fitzpatrick, E., *Correcting for the Effects of Interstellar Extinction*, PASP, 111, 63-75, 1999.
- García-Burillo, S., Sempere, M., Bettoni, D. *First Detection of a Counter rotating Molecular Gas Disk in a Spiral Galaxy: NGC 3626*, ApJ, 502, 235-244, 1998

- George, M., Chung-Pei, M., Bundy, K. et al. *Galaxies in X-ray Groups. III. Satellite Color and Morphology Transformations*, arXiv:astro-ph/1302.6620, 1-11, 2012
- Gil de Paz, A., Boissier, S., Madore, B., et al. *The GALEX Ultraviolet Atlas of Nearby Galaxies*, ApJS, 173, 185-255, 2007
- Grossi, M., di Serego Alighieri, S., Giovanardi, C. et al., *The HI content of early-type galaxies from the ALFALFA survey. II. The case of low density environments*, A&A 498, 407-417, 2009
- Haynes, M., Jore. K., Barrett, E., et al. *Kinematic Evidence of Minor Mergers in Normal SA Galaxies: NGC 3626, NGC 3900, NGC 4772, and NGC 5854*, ApJ, 120, 703-727, 2000.
- Hopkins, A., Miller, C., Nichol, A., et al. *Star Formation Rate Indicators in the Sloan Digital Sky Survey*, ApJ, 599, 971-991, 2003
- Kawata, D., Mulchaey, J.S, *Strangulation in galaxy groups*, ApJ, 672, L103-L106, 2008
- Horellou, C., Black, J. H., van Gorkom, J. H., Combes, F., van der Hulst, J. M., Charmandaris, V., *Atomic and molecular gas in the merger galaxy NGC 1316 (Fornax A) and its environment*, A&A, 376, 837-852, 2001
- Hughes, T.M., Cortese, L. *The migration of nearby spirals from the blue to the red sequence: AGN feedback or environmental effects?*, MNRAS, 396, L41-L45, 2009
- Kroupa, P. *The Dark Matter Crisis: Falsification of the Current Standard Model of Cosmology*, PASA, 29, 395-433, 2012
- Jedrzejewski R. I., *CCD surface photometry of elliptical galaxies. I - Observations, reduction and results*, MNRAS, 226, 747-768, 1987
- Just, D. W., Zaritsky, D., Sand, D. J., Desai, V., Rudnick, G., *The Environmental Dependence of the Evolving S0 Fraction*, ApJ, 711, 192-200, 2010
- Laurikainen, E., Salo, H., & Buta, R., *Multicomponent decompositions for a sample of S0 galaxies*, MNRAS, 362, 1319-1347, 2005.

- Laurikainen, E., Salo, H., & Buta, R., *Morphology of 15 southern early-type disk galaxies*, ApJ, 132, 2634-2652, 2006.
- Lewis, I., Balogh, M., De Propris, R., Couch, W., et al., *The 2dF Galaxy Redshift Survey: the environmental dependence of galaxy star formation rates near clusters*, MNRAS, 334, 673-683, 2002
- Martin, C., Wyder, T., Schiminovich, D., et al., *The UV-optical galaxy color-magnitude diagram. III. Constraints on evolution from the blue to the red sequence*, ApJS, 173, 342-356, 2007.
- Marino, A., Rampazzo, R., Bianchi, L., et al., *Galaxy evolution in nearby loose groups. II. Photometric and kinematic characterization of USGC U268 and USGC U376 group members in the Leo cloud*, MNRAS, 428, 476-501, 2013
- Marino, A., Bianchi, L., Rampazzo, R., et al., *Tracing rejuvenation events in nearby S0 galaxies*, ApJ, 736, 154-162, 2011a
- Marino, A., Rampazzo, R., Bianchi, L., et al., *Nearby early-type galaxies with ionized gas: the UV emission from GALEX observations*, MNRAS, 411, 311-331, 2011b
- Mazzei, P., Xu, C., & de Zotti, G., *A model for the photometric evolution of disc galaxies from UV to far-IR*, A&A, 256, 45-55, 1992.
- Mazzei, P. & De Zotti, G., Xu, C., *Models for the evolution of the spectral energy distribution of elliptical galaxies from ultraviolet to far-IR wavelengths*, ApJ, 422, 81-91, 1994.
- Mazzei, P. & De Zotti, G., *The far-IR properties of early-type galaxies*, ApJ, 426, 97-104, 1994.
- Mazzei, P. *The history of star formation in galaxies. Insights from SPH simulations of triaxial collapsing systems*, Mem. Sait, 74, 498-499, 2003.
- Mazzei, P. & Curir, A., *Dark and luminous matter connections from smooth particle hydrodynamics simulations of isolated collapsing triaxial systems*, ApJ, 591, 784-790, 2003: MC03

- Mazzei, P., *Dark and luminous matter connections. Toward understanding galaxy evolution*, Research Signpost, Recent Res. Devel. Astron. & Astrop., 1, 457-473, 2003, (arXiv:astro-ph/0401509)
- Moiseev, A., Bizyaev, D., *3D spectroscopic study of galactic rings: Formation and kinematics*, New Astron. Rev., 53, 169-174, 2009
- Navarro, J., Frenk, C., White, S., *A Universal Density Profile from Hierarchical Clustering*, ApJ, 490, 493-508, 1997
- Paturel G., Petit C., Prugniel P., et al. *HYPERLEDA. I. Identification and designation of galaxies*, A&A, 412, 45-55, 2003
- Phillipps, S., Disney, M., *The surface brightness of spiral galaxies. I - Spheroidal components and Freeman's law*, MNRAS, 203, 55-65, 1983
- Ramella, M., Geller, M., Pisani, A., da Costa L., *The UZC-SSRS2 Group Catalog*, AJ, 123, 2976-2984, 2002
- Rampazzo, R., Panuzzo, P., Vega, O. et al. *A Spitzer-IRS spectroscopic atlas of early-type galaxies in the Revised Shapely-Ames Catalog* MNRAS, in press. (DOI 10.1093/mnras/stt475)
- Rifatto, A., Longo, G., Capaccioli, M., *The UV properties of normal galaxies. III. Standard luminosity profiles and total magnitudes*, A&A Sup. Ser., 114, 527-536, 1995
- Ryan-Weber, E., Webster, R., Staveley-Smith, L. *The 1000 Brightest HIPASS galaxies: The HI mass function and Ω_{HI}* , MNRAS, 343, 1195-1206, 2003
- Salpeter, E.E., *The Luminosity Function and Stellar Evolution.*, ApJ, 121, 161-167, 1955
- Salim, S., Charlot, S., Rich R.M., et al. *New constraints on the star formation History and dust attenuation of galaxies in the local Universe from GALEX* ApJ, 619, L39-L42, 2005
- Salim, S., Fang, J. J., Rich, R.M. et al. *Galaxy-scale star formation on the red sequence: the continued growth of S0s and the quiescence of ellipticals* ApJ, 755, 105(pp.29), 2012

- Sandage, A., Tammann, G. A. *A revised Shapley-Ames Catalog of bright galaxies*, Carnegie Institution of Washington Publication, Washington: Carnegie Institution 2nd edition, 1987 (RSA)
- Schawinski, K., Kaviraj, S., Khochfar, S. et al., *The Effect of Environment on the Ultraviolet Color-Magnitude Relation of Early-Type Galaxies*, ApJS, 173, 512-523, 2007
- Schawinski, K., Virani, S., Simmons, B., Urry, M.C., Treister, E., Kaviraj S., Kushkuley, B. *Do moderate-luminosity active galactic nuclei suppress star formation?* ApJ, 692, L19-L23, 2009
- Serra, P., Oosterloo, T.A. *Cold gas and young stars in tidally disturbed ellipticals at $z = 0$* , MNRAS, 401, L29L33, 2010
- Silchenko, O., Moiseev, A., & Shulga, A. , *Lenticular galaxies at the outskirts of the Leo II group: NGC 3599 and NGC 3626*, AJ, 140, 1462-1474, 2010.
- Spavone, M., Iodice, E., Calvi, R., Bettoni, D., Galletta, G., Longo, G., Mazzei, P. & Minervini, G. *Revisiting the formation history of the minor-axis dust lane galaxy NGC 1947*, MNRAS, 393, 317-328, 2009
- Spavone, M., Iodice, E., Bettoni, D., Galletta, Mazzei, P. & Reshetnikov, V., *A new photometric investigation of the double-ringed galaxy ESO 474-G26: unveiling the formation scenario*, MNRAS, 426, 2003-2018, 2012
- Strateva, I., Ivezić, Knapp, et al. *Color separation of galaxy types in the Sloan Sky Survey imaging data*, AJ, 122, 1861-1874, 2001
- Temi, P., Brighenti, F., Mathews, W., *SPITZER observations of passive and star-forming early-type galaxies: an infrared color-color sequence*, ApJ, 707, 890-902, 2009
- Thilker, D. A., Bianchi, L., Meurer, G. et al. *A search for extended ultraviolet disk (XUV-disk) galaxies in the local Universe*, ApJS, 714, 538-571, 2007
- Thilker, D. A., Bianchi, L., Schiminovich, D. et al. *NGC 404: A Rejuvenated Lenticular Galaxy on a Merger-induced, Blueward Excursion Into the Green Valley*, ApJ, 714, L171-L175, 2010

- Villalobos, A., De Lucia, G., Borgani, S, Murante, G. *Simulating the evolution of disc galaxies in group environment.I. The influence of the global tidal field*, MNRAS, 424, 2401-2428, 2012
- Warren, M., Quinn, P., Salmon, J. & Zurek, W. *Dark halos formed via dissipationless collapse. I - Shapes and alignment of angular momentum*, ApJ, 399, 405-425, 1992
- Weijmans, A-M., Krajnovič, D., van de Ven, G. et al., *The shape of the dark matter halo in the early-type galaxy NGC 2974*, MNRAS, 383, 1343-1358, 2008
- Werk, J, Putman, M, Meurer, G. et al. *Outlying HII regions in HI-selected galaxies*, AJ, 139, 279-295, 2010.
- Wetzel, A., Tinker, J., Conroy, C. et al. *Galaxy evolution in groups and clusters: satellite star formation histories and quenching timescales in a hierarchical Universe*, MNRAS, 1-24, 2012
- Wilman, D. J., Oemler, A., Mulchaey, J. S., McGee, S. L., Balogh, M. L., Bower, R. G., *Morphological Composition of $z \approx 0.4$ Groups: The Site of S0 Formation*, ApJ, 692, 298-308, 2009
- Wyder, T., Martin, K., Schiminovich, D. et al, *The UV-Optical Galaxy Color-Magnitude Diagram. I. Basic Properties*, ApJSS, 173, 293-314, 2007
- Yamamura, I., Makiuti, S., Ikeda, N., et al. *The first release of the AKARI/FIS Bright source catalogue*, AIP Conf. Proc. *The exoplanets and disks: their formation and diversity*, 1158, 169-170, 2009